Electron–Phonon Coupling in CdSe/CdS Core/Shell Quantum Dots

ARTICLE *in* ACS NANO · JULY 2015

Impact Factor: 12.88 · DOI: 10.1021/acsnano.5b02230 · Source: PubMed

4 AUTHORS, INCLUDING:

Ke Gong

University of California, Merced

16 PUBLICATIONS **44** CITATIONS

SEE PROFILE

Electron–Phonon Coupling in CdSe/CdS Core/Shell Quantum Dots

Chen Lin, Ke Gong, David F. Kelley,* and Anne Myers Kelley*

Chemistry and Chemical Biology, University of California, Merced, 5200 North Lake Road, Merced, California 95343, United States

ABSTRACT Resonance Raman spectra and excitation profiles have been measured and semiquantitatively modeled for core/shell quantum dots consisting of 2.7 nm diameter zincblende CdSe cores and thin (0.5 nm) or thick (1.6 nm) CdS shells. The Raman spectra show previously reported trends of increased peak frequency for both the CdSe and the CdS longitudinal optical (LO) phonons with increasing shell thickness. We also find a strong dependence of the peak CdS frequency on excitation energy and a large discrepancy between the experimental frequency of the CdSe + CdS combination band and the sum of the corresponding fundamental frequencies. This suggests that the dominant transitions at high excitation energies are localized on either the CdSe core or the CdS shell and thereby cannot enhance combination band transitions between core and shell. The CdS to CdSe Raman intensity ratios at high excitation energies further support this picture. The electron–phonon coupling for the CdSe LO phonon in the lowest excitonic transition is slightly weaker in the core/shell structures than in pure CdSe quantum dots, contrary to expectations for the Fröhlich coupling mechanism. Possible explanations for this discrepancy are discussed.

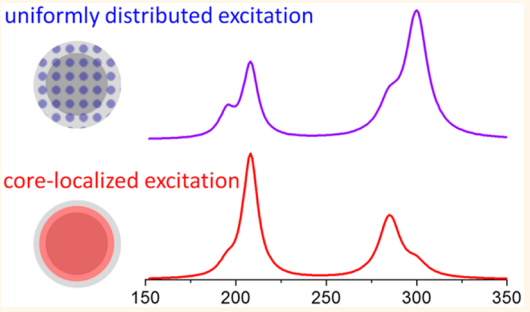

KEYWORDS: core/shell · quantum dot · electron–phonon coupling · Fröhlich · resonance Raman

Semiconductor nanocrystals consisting of a core of one material and one or more shells of different materials are widely studied. Core/shell structures afford greater diversity in spectroscopic, photophysical, and chemical properties than can be obtained from single-component nanocrystals, and methods for synthesizing well-defined core/shell structures are well developed. A number of recent papers have addressed the optical properties of structures consisting of a CdSe core and a CdS shell, sometimes with a second, outer shell of ZnS to confer additional chemical stability.[1−30] The lattice mismatch between CdSe and CdS is about 4%, allowing thin shells of CdS to be grown epitaxially with lattice strain on CdSe cores. The CdSe/CdS combination is also interesting because it is an example of a so-called "type I 1/2" or "quasi-type II" heterostructure; the conduction bands of CdSe and CdS are nearly aligned, while the valence band of CdSe is considerably above that of CdS, so it is energetically favorable for the hole to remain localized in the CdSe core while the electron is delocalized over the entire structure.[11,31]

The phonons of CdSe/CdS nanocrystals have been studied by a number of groups using both direct electronic spectroscopy (emission/emission excitation)[2,7,32] and Raman spectroscopy.[1,10,15,22] Low-temperature electronic spectroscopy on single nanocrystals reveals resolved phonon modes whose intensities give the electron–phonon coupling strengths for the 1S–1S excitonic transition. Raman spectroscopy has been used mainly to examine alloying at the CdSe/CdS interface and the existence of lattice strain in core and/or shell resulting from the lattice mismatch. The Raman intensities, particularly the intensity ratios of overtone transitions to fundamentals, also depend on the magnitude of electron–phonon coupling (EPC), but this information is complicated to extract and generally requires Raman excitation profiles and absolute scattering cross sections[33] which are not part of the analyses presented to date on core/shell QDs.

In recent work, we measured and quantitatively modeled the resonance Raman excitation profiles of organic ligand capped CdSe quantum dots (QDs) in solution in order to obtain the electron–phonon

* Address correspondence to amkelley@ucmerced.edu, dfkelley@ucmerced.edu.

Received for review April 14, 2015 and accepted July 25, 2015.

Published online July 26, 2015
10.1021/acsnano.5b02230

coupling strengths and their dependence on QD size.[34,35] The EPC for the dominant longitudinal optical (LO) mode of CdSe was found to be nearly independent of QD size from 2.6 to 5.2 nm diameter. The size independence of the EPC and its order of magnitude were reproduced through calculations combining an atomistic model for the phonons with a two-band effective mass model for the electron and hole wave functions.[35] In these calculations, the EPC was assumed to arise from the Fröhlich mechanism, the interaction between the electric field generated by the exciton and the oscillating dipole created by the phonon. The Fröhlich mechanism is generally assumed to be the dominant source of electron–phonon coupling in polar crystals.[36,37]

Here, we extend these studies to CdSe/CdS core/shell QDs with shells of two different thicknesses. It is our expectation that the greater degree of charge separation in this core/shell system, with the hole localized to the core and the electron delocalized over both core and shell, should induce a larger exciton–phonon coupling for the CdSe phonons and provide a more sensitive test of the Fröhlich mechanism. Resonance Raman excitation profiles obtained over a wide range of excitation wavelengths (spanning more than 5000 cm^{-1} in energy) also allow us to probe the state dependence of the exciton–phonon coupling for both CdSe and CdS phonon modes.

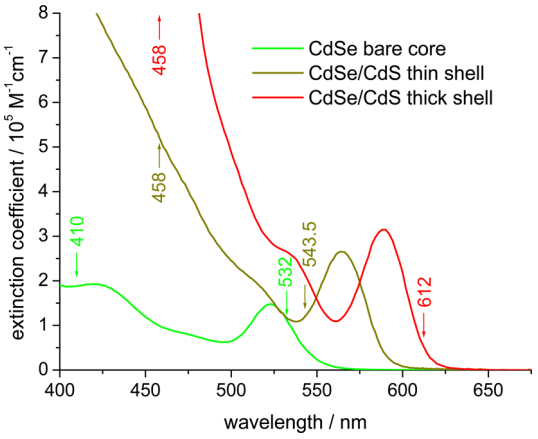

Figure 1. Optical absorption spectra for the three samples studied, and the shortest and longest Raman excitation wavelength used for each sample.

RESULTS

Figure 1 shows the optical absorption spectra of the bare cores and the two core/shell samples examined. The molar extinction coefficients were assigned such that the integrated area of the lowest excitonic absorption matched those of ref 38, which in turn were scaled to the absorbance at 350 nm. This figure also shows the range of excitation wavelengths used for each sample.

Figure 2 shows representative Raman spectra of the three samples obtained with excitation near the lowest excitonic absorption and at two shorter wavelengths having comparable energies above the lowest exciton for each sample. All of the spectra show the fundamental of the CdSe LO phonon near 207 cm^{-1}, and the core/shell structures also show the fundamental of the CdS LO phonon in the 285–300 cm^{-1} range. The CdSe LO phonon shifts up in frequency by several cm^{-1} between the bare cores and the thicker shells. This has been observed by other workers (see Discussion) and is attributed to compression of the core by the shell. The relative intensity of the CdS LO phonon is much larger in the thick-shelled samples, which contain a higher fraction of CdS, and it is also much larger at shorter wavelengths for both samples. The overtone of the CdSe LO phonon appears in the spectra near 410 cm^{-1}, as does the combination band transition (one quantum each of CdSe and CdS LO phonons) near 490 cm^{-1}

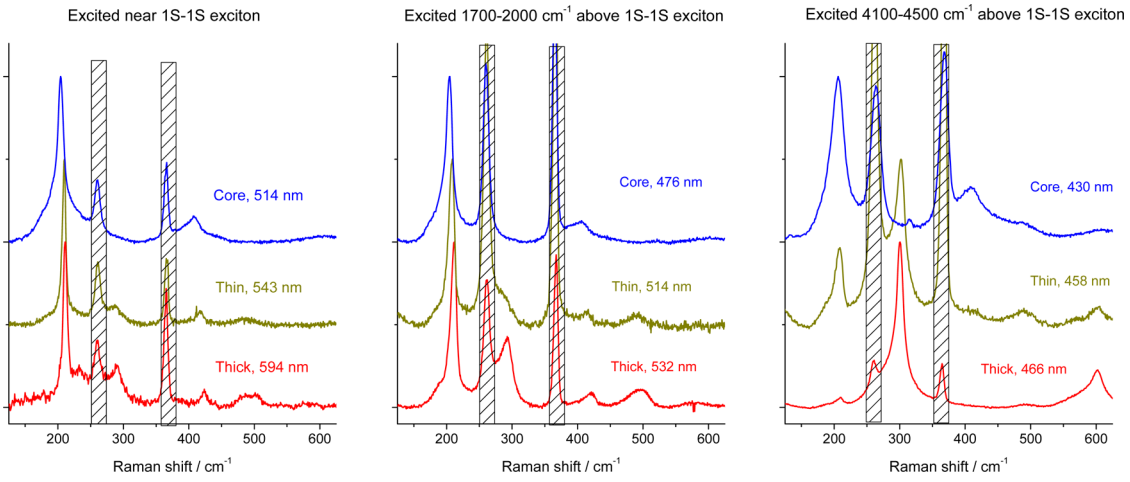

Figure 2. Resonance Raman spectra of bare CdSe cores (blue), CdSe cores with thin CdS shells (dark yellow), and CdSe cores with thick CdS shells (red), excited near the first excitonic absorption (left), 1700–2000 cm^{-1} to the blue (middle), and 4100–4500 cm^{-1} to the blue (right). The black hatched bars cover the two strong chloroform solvent lines, whose relative intensity varies strongly with QD concentration and resonance condition.

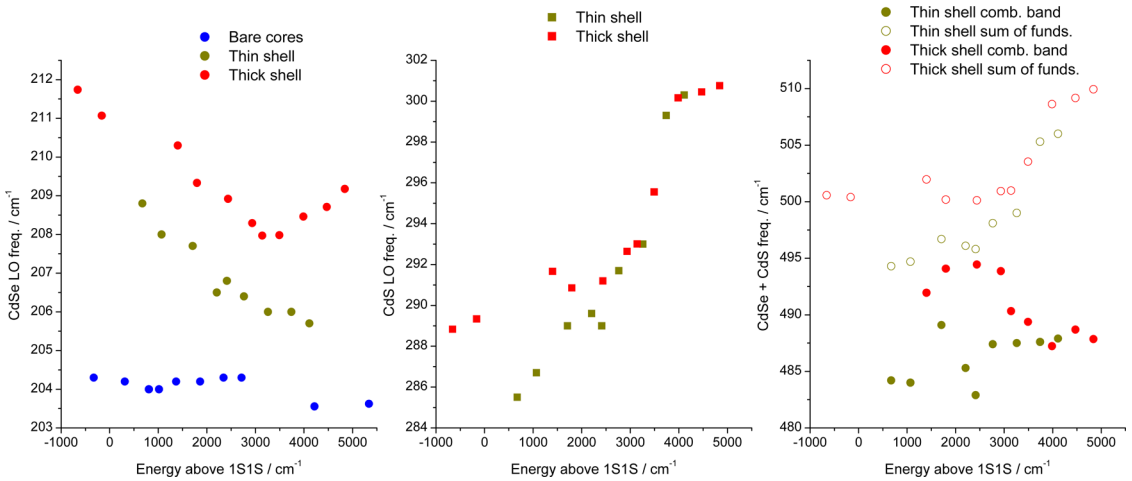

Figure 3. Frequency of CdSe LO phonon (left), CdS LO phonon (center), and CdSe + CdS combination band (right) as a function of excitation energy above the first excitonic transition. Bare cores, CdSe/CdS thin shells, and CdSe/CdS thick shells are plotted in blue, dark yellow, and red, respectively. The right-hand plot compares the actual combination band frequency (solid dots) to the sum of the two fundamental peak frequencies (open circles).

in the core/shell structures. The appearance of the combination band demonstrates that there are resonant excitonic transitions involving both the CdSe core and the CdS shell. Oddly, however, even the thick-shelled CdSe/CdS structures show little or no intensity in the overtone of the CdS LO phonon, near 600 cm^{-1}, except at the highest excitation energies. The CdSe LO overtone to fundamental ratio is in the 0.1−0.2 range for both thin and thick shells except at the highest excitation energies, where it increases significantly. This is somewhat lower than the LO overtone intensity observed in pure CdSe NCs.[34,39]

The frequencies of the Raman lines in the core/shell structures also display a significant dependence on the resonance condition. Figure 3 plots the frequencies of each of the fundamentals and the combination band as a function of energy above the lowest excitonic transition for all three samples. In the bare cores, the CdSe frequency varies with excitation wavelength by a maximum of about 1 cm^{-1}, appearing to shift to slightly lower frequency at the highest excitation energies. In the CdSe/CdS structures, the CdSe frequency increases with increasing shell thickness but also varies by 3−4 cm^{-1} as the excitation energy is varied. The CdS LO frequency shows a much more pronounced variation, increasing by as much as 15 cm^{-1} as the excitation is tuned to shorter wavelengths. The CdSe + CdS combination band mode appears at a frequency 5−20 cm^{-1} lower than the sum of the fundamentals and its frequency does not vary with excitation energy in the same way as the fundamentals, as shown in the right-hand panel of Figure 3 which compares the measured frequency to the sum of the fundamental frequencies. (In contrast, the overtone frequencies, where the overtones are clearly observed, are within 4 cm^{-1} of twice the fundamental frequency.) Some of these trends were previously reported by others, but those data were incomplete because fixed excitation wavelengths were used. The frequency of the CdS LO phonon has been reported to increase by anywhere from 6 to 24 cm^{-1} upon increasing the shell thickness in CdSe/CdS core/shell structures.[1,10,15,22] Most studies on CdSe/CdS core/shells also report that the CdSe LO fundamental shifts to higher frequencies by 3−7 cm^{-1} between bare CdSe cores and thick CdS shells. Most of the previously reported Raman spectra for CdSe/CdS core/shell structures show significant intensity in the CdS overtone, but in all cases these spectra were excited >3500 cm^{-1} above the lowest exciton.[10,15,25] The one exception was the study by Lu *et al.* using 514.5 nm excitation,[1] where the CdS overtone is essentially undetectable for shell thicknesses of 3.5 layers or less (energy <2800 cm^{-1} above the lowest exciton) but suddenly becomes quite intense for 5.5 layer shells (∼3200 cm^{-1} above the lowest exciton). These results are all consistent with our observation that the CdS overtone appears only at high excess energies.

Figure 4 plots the Raman cross sections for the CdSe and CdS fundamentals in the core/shell structures as a function of excitation energy above the lowest excitonic peak. Both of the fundamentals are enhanced at the lowest excitonic peak, as expected for an excitation in which the electron is delocalized over the entire QD. However, at higher energies the CdS band shows additional enhancement, particularly for the thicker shells, while the CdSe cross-section remains low despite the strong absorption in this region. In our thin-shelled samples (2.7 nm diameter core, 0.5 nm shell), about 61% of the particle volume is CdS, while the thick-shelled samples (2.7 nm diameter core, 1.6 nm shell) are about 90% CdS by volume. One might expect that if the resonant excitonic transitions were evenly distributed throughout the nanocrystal, the Raman intensities of the CdSe and CdS LO phonons should

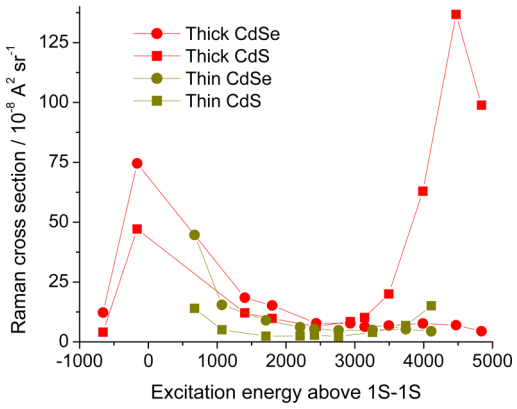

Figure 4. Raman cross section for the CdSe (circles) and CdS (squares) LO phonon fundamentals as a function of excitation energy above the lowest excitonic absorption peak for thick-shelled and thin-shelled CdSe/CdS core/shell QDs. Values are for parallel polarization only.

be proportional to the volume fractions scaled by the usual ω^2 dependence of resonance Raman intensities on vibrational frequency.[40] This would give a CdSe:CdS intensity ratio of roughly 1:3 for the thin shells and 1:20 for the thick shells. Experimentally, we find that at excitation energies near the first excitonic origin the thin-shelled samples actually show a CdSe:CdS intensity ratio of around 3:1, while for the thick shells, it is about 3:2, qualitatively consistent with the lowest-energy, 1S−1S exciton being largely localized to the CdSe core. At the highest-energy excitations, the CdSe:CdS intensity ratios are very close to the expected 1:3 and 1:20 for thin and thick shells, respectively. This suggests that the higher-energy excitations are either almost uniformly delocalized over the entire QD or consist of a large number of more localized excitations, equally distributed throughout the core and the shell, that are close in energy.

DISCUSSION

CdS Modes and CdSe + CdS Combination Bands. In a resonance Raman process, the Raman shift is indicative of the ground state phonon frequency, and the Raman shift for a particular transition does not depend on the resonance condition. However, the experimental Raman spectra show significant variations in the CdSe and CdS LO phonon fundamental frequencies with changes in the excitation wavelength (Figure 3). The largest variations are seen in the case of the CdS LO phonon. Comparison of the thin and thick shell spectra shows that these variations cannot be explained in terms of sample heterogeneity. The CdS frequency difference between the thin and thick shell particles is, at most, about 3 cm^{-1}. This is much smaller than the 12 cm^{-1} variation seen with excitation frequency. Furthermore, if there were considerable particle to particle shell thickness inhomogeneity, we would not have the well resolved exciton peak in Figure 1. We also note that the effect of shell thickness inhomogeneity on the Raman frequencies goes in the wrong direction to explain the observed result. QDs with thicker shells generally show higher CdS phonon frequencies but also absorb at longer wavelengths, and both the CdSe and CdS Raman transitions undergo considerable enhancement on resonance with the lowest excitonic transition. If the sample consisted of a broad range of shell thicknesses, we would expect the observed CdS phonon frequency to increase with longer-wavelength excitation, as the thicker-shelled QDs are preferentially enhanced, rather than decrease. We conclude that the observed variation of the CdS LO frequency with excitation wavelength is intrinsic to CdSe/CdS core/shell QDs.

At least three possible origins can be considered for the large discrepancy between the frequency of the CdSe + CdS combination band and the sum of the two fundamental frequencies. One is simple vibrational anharmonicity. For our core/shell NCs, the anharmonicities as evidenced by the overtone frequencies are quite small; the overtones of the CdSe and CdS LO phonons are within ~1% of the fundamental frequencies. To explain the combination band data, one would have to postulate that the anharmonic coupling between the CdSe and CdS LO phonons is very large even though the diagonal anharmonicity of each mode separately is small. This cannot be excluded, but there is no obvious mechanism by which this would occur, so it seems unlikely. A second possibility is that our sample contains, in addition to CdSe/CdS core/shell structures, some pure CdS nanocrystals formed by homogeneous nucleation during shell growth. Structures containing only CdS would have a strong CdS LO phonon but would not produce any combination bands with CdSe phonons. This possibility can be excluded by the absence of any significant fluorescence in unquenched samples excited in the 514–458 nm region. The third, and most likely, explanation for the combination band frequency anomaly is that the CdSe and/or CdS LO phonon regions consist of a number of different normal modes with slightly different frequencies that are resonance enhanced through different excitonic transitions. Since resonance Raman intensity in a combination band requires that both modes be enhanced through the same resonant transition, this mechanism would allow only particular pairs of CdSe/CdS modes to show up as combination bands, possibly at a considerably different frequency from the average of the fundamentals.

The variation of the CdS and CdSe + CdS combination phonon frequencies can be understood in terms of the spatial extent of these modes and the excitations that enhance them in the Raman spectra. We have discussed the makeup of the "LO phonon" mode in pure CdSe QDs,[41,42] and it is reasonable to expect that the CdS LO phonon also consists of many different modes having slightly different frequencies. Indeed,

the breadth and asymmetry of the CdS "LO phonon" clearly shows that it is composed of multiple normal modes. These normal modes can also have different spatial distributions. This is important because the Raman activity of a particular phonon mode is partially determined by the spatial overlap between the phonon and the resonant exciton, and the spatial extent of the exciton varies with excitation wavelength. If the incident light is resonant with the lowest exciton, then the Raman modes that are active will be those that overlap the 1S−1S exciton. The 1S electron and hole wave functions (particularly the hole) are strongly peaked in the center of the particle, and have decreasing density with increasing radius through the shell.[31] In contrast, shorter wavelength excitation is resonant or near-resonant with a number of different excitons that are localized in different regions of the QD but are, on average, more equally distributed between core and shell. Thus, light resonant with the lowest exciton is expected to produce comparatively greater Raman intensity in core phonon modes and shell phonon modes that are closer to the core/shell interface.

Several lines of reasoning suggest that the higher-frequency components of the CdS LO phonon involve mainly motions of atoms farther away from the interface with the CdSe core. Near the CdSe interface, the lattice mismatch between the two materials tends to expand the CdS lattice, leading to a decrease in vibrational frequency for those CdS-type modes having large contributions from the atoms near the interface. Consistent with this expectation, surface-enhanced Raman spectra of CdS/CdSe superlattices show that the CdS LO phonon is shifted by 15−25 cm^{-1} to lower frequency near an interface with CdSe.[43] The higher frequency CdS modes arise from areas of the shell that are less affected by the lattice strain induced by the interface (both pure CdS QDs[44−46] and bulk CdS[46,47] exhibit peak Raman frequencies of 300−305 cm^{-1} at room temperature, close to the 300−301 cm^{-1} we measure at high excitation energies) and these modes are more effectively resonance enhanced by excitations that are largely localized to the CdS shell. Although a strain mechanism is surely operative, elastic continuum calculations[48] suggest that this effect is too small to explain all of the excitation wavelength dependence of the CdS LO phonon. Furthermore, elastic continuum calculations indicate that the volumetric strain in the shell varies only slowly with the radial coordinate. These calculations are consistent with the qualitative notion that if lattice strain were the only thing determining these frequency shifts, the shift of the CdSe mode to higher frequency should be approximately equal to the CdS shift to lower frequency. The observation that the CdS shift is much larger suggests that there must be other mechanisms involved. We note that because the CdS shell is deposited at low temperature (∼140 °C), alloying at the core/shell interface should be minimal. However, even at a physically sharp interface, the lattices of both core and shell materials will be distorted and the phonon modes at the interface may involve a mixture of Se and S motions, thereby appearing at a lower frequency than a pure CdS phonon. We therefore suggest that most of the shift to lower frequencies is due to mode mixing. CdS vibrations that are localized near the interface are mixed with CdSe modes, resulting in an overall lower frequency phonon. These lower frequency, interface localized modes are preferentially active following excitation of the lowest exciton, resulting in the observed behavior in Figure 3.

To test this hypothesis, we simulated the Raman spectra and excitation profiles[34] using a minimal model in which the CdSe and CdS "LO phonons" are each composed of two modes having different frequencies. The higher-frequency CdSe mode is coupled only to the lowest-energy exciton ($1S_e1S_{3/2}$), while the lower-frequency mode is coupled to higher-lying excitonic states, consistent with our previous analysis of the CdSe LO phonon band shape.[42] The high-frequency CdS mode is assumed to be coupled mainly to a transition about 5000 cm^{-1} above the lowest exciton in the near-continuum absorption region, while the lower-frequency mode is coupled to the lower-energy excitonic transitions. Figures 5 and 6 show the calculated excitation profiles for the fundamentals, overtones, and combination band, while Figure 7 shows the calculated frequencies for the fundamentals and the combination band. The parameters employed are collected in Table 1. The fitting parameters for the higher-lying excitations in particular should not be taken too literally because little is known about the numbers and positions of the excitonic transitions in this region. Also, in order to reduce the number of parameters and simplify the calculations,[34,35] the fine-structure splitting was ignored and all transitions were assumed to be polarized in the same direction. The calculations consistently underestimate the total intensity in the CdSe + CdS combination band region, particularly for the thin-shelled samples. However, the semiquantitative fits obtained, particularly for the thicker-shelled QDs, support this explanation for the decrease in CdSe fundamental frequency and increase in CdS frequency with increasing excitation energy. The calculations also qualitatively reproduce the noncoincidence between fundamental and combination band frequencies.

Our results indicate that much of the absorption in the region >4000 cm^{-1} above the lowest excitonic absorption band involves transitions that are essentially localized to either the CdSe core or the CdS shell. Calculations of the electron and hole wave functions using the effective mass approximation envelope function model[41,42,49] do not predict any such localization; the hole wave functions are largely core-localized at

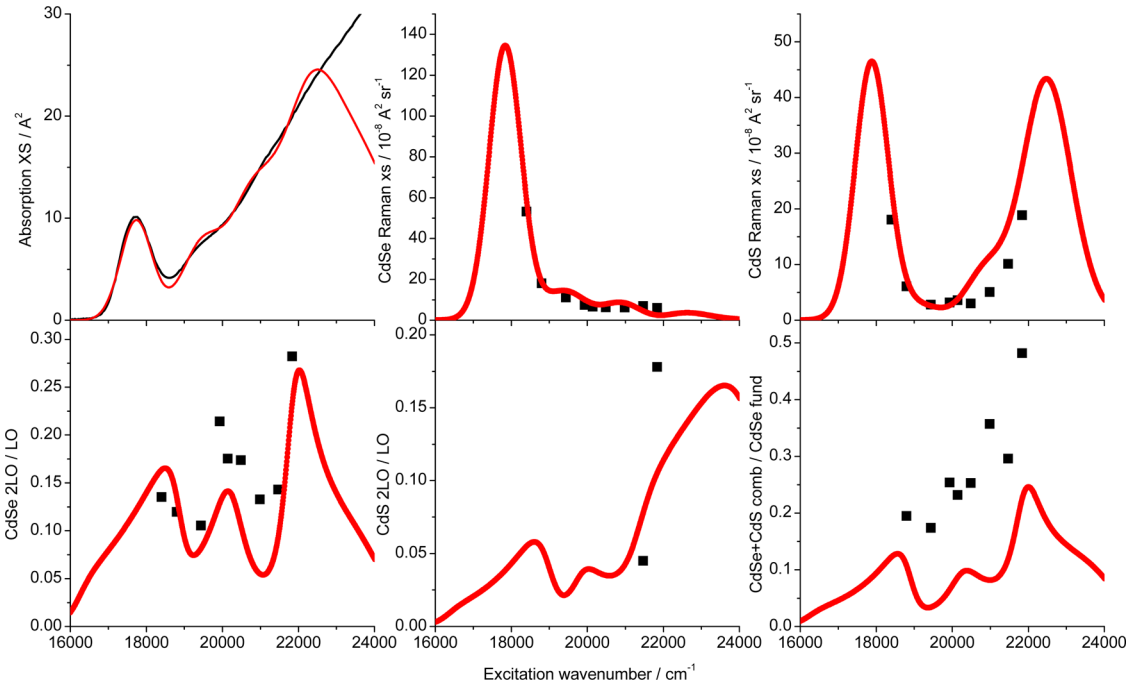

Figure 5. For thin-shelled CdSe/CdS core/shell QDs, calculated absorption spectrum (upper left), CdSe and CdS Raman fundamental cross sections (upper middle and right), CdSe and CdS Raman overtone intensity ratios to fundamental (lower left and middle), and CdSe + CdS combination band intensity ratio to CdSe fundamental (lower right). All calculations use the parameters of Table 1.

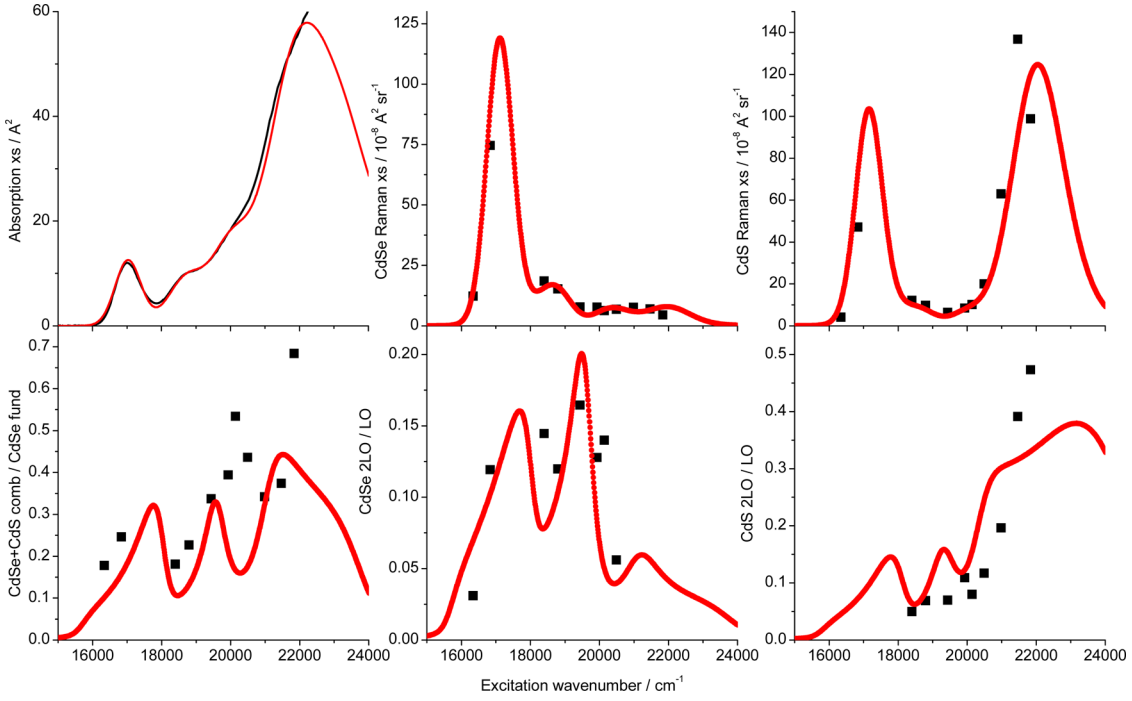

Figure 6. Same as Figure 5, for thick-shelled CdSe/CdS QDs.

low energies and delocalized at higher energies, while the electron wave functions are all delocalized over both core and shell owing to the small conduction band offset between CdSe and CdS. This suggests that the effective mass approximation particle-in-a-sphere model does not given an appropriate description of the higher-energy excitations, which should not be surprising given the assumption of parabolic bands inherent to this model. Qualitative discrepancies between the predictions of the effective mass model and results from quantum chemical calculations have been described previously.[50,51] The idea that highly energetic electron–hole pairs are bulk-like and largely localized on a length scale smaller than that of the

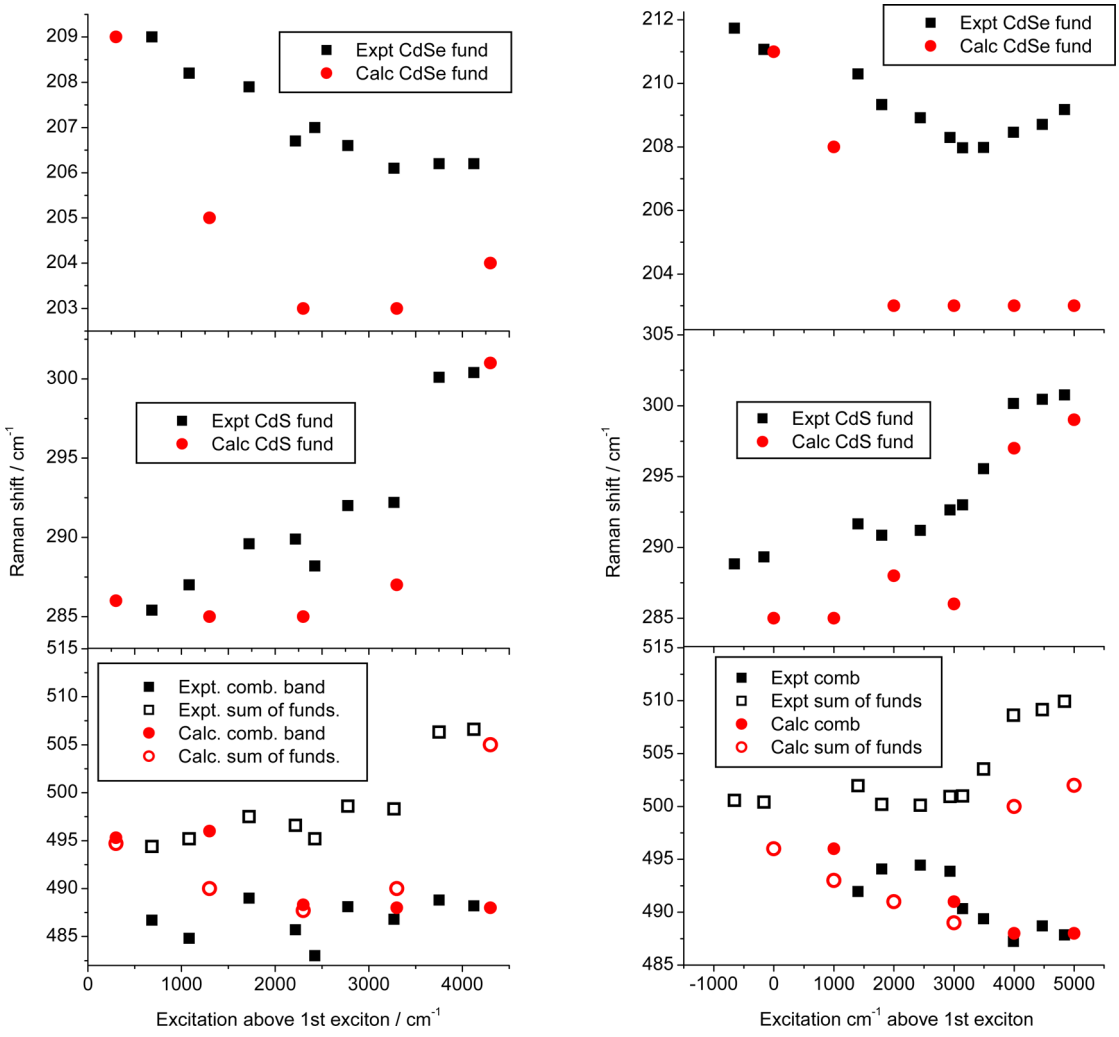

Figure 7. Experimental (black) and calculated (red) frequencies for CdSe fundamental (top), CdS fundamental (middle), and CdSe + CdS combination band (bottom), for thin-shelled (left) and thick-shelled (right) CdSe/CdS QDs. Open symbols in bottom plot are the sum of the fundamental peak frequencies.

TABLE 1. Parameters used for simulation of Raman excitation profiles and spectra

Thin Shell, Inhomogeneous Width = 880 cm^{-1}						
energy/cm^{-1}	homog. width/cm^{-1}	trans. length/Å	S (CdSe, 203 cm^{-1})	S (CdSe, 209 cm^{-1})	S (CdS, 285 cm^{-1})	S (CdS, 300 cm^{-1})
17730	350	3.0	0	0.125	0.03	0
19450	850	2.75	0.24	0	0.03	0
20750	1000	3.15	0.18	0	0.08	0
22000	1000	1.7	0.98	0	0.28	0
22300	1000	2.6	0	0	0	0.4
23100	3000	6.5	0	0	0	0

Thick Shell, Inhomogeneous Width = 750 cm^{-1}						
energy/cm^{-1}	homog. width/cm^{-1}	trans. length/Å	S (CdSe, 203 cm^{-1})	S (CdSe, 211 cm^{-1})	S (CdS, 285 cm^{-1})	S (CdS, 300 cm^{-1})
17030	350	3.29	0	0.125	0.08	0
18700	850	3.05	0.32	0	0.08	0.045
19950	1000	3.5	0.125	0	0.08	0.045
21700	1000	3.0	0.18	0	0.5	0
22000	1000	3.0	0	0	0	2.0
22600	3000	10.5	0	0	0	0

quantum dot has been put forward previously for PbS[52] and PbSe[53] QDs. Experiments on CdSe/CdS dot-in-rod structures have also been interpreted to show long-lived exciton localization in the CdS shell.[20,23,29]

Mechanism and Magnitude of Electron−Phonon Coupling. Both the bulk band offsets and a wealth of experimental evidence indicate that, in CdSe/CdS core/shell QDs, the lowest excitonic transition involves a hole that is largely localized to the CdSe core and an electron that is fairly delocalized throughout the core and shell ("type I 1/2" or "quasi-type II"). Compared with pure CdSe QDs, where there is only a small amount of spatial separation between electron and hole, the lowest excitonic state of the core/shell structures should involve considerably larger internal electric fields and, therefore, stronger coupling to polar optical phonons through the Fröhlich mechanism. Calculations on core/shell structures using methods similar to those described in ref 35 (an atomistic model for the phonons, a two-band effective mass model for the electron and hole wave functions, and Fröhlich coupling) are shown in Supporting Information. These calculations predict that the Huang−Rhys parameters for the CdSe LO phonons should be factors of 1.8−2.6 larger for CdSe/CdS core/shell QDs than for the CdSe cores. However, for CdSe/CdS QDs we find (Table 1) a Huang−Rhys parameter of about 0.125 for the CdSe LO phonon in the $1S_e1S_{3/2}$ state, compared with 0.18−0.24 for pure CdSe QDs in the 2.6−5.2 nm size range.[35] The result of somewhat weaker EPC for the core/shell structures compared with bare cores appears quite robust with regard to changes in the modeling assumptions, *e.g.*, inclusion of the fine-structure splitting needed to reproduce the Raman depolarization ratios[34,35] (see Supporting Information). The weaker electron−phonon coupling in the core/shell structure is hard to reconcile with a predominantly Fröhlich mechanism. Furthermore, CdSe/ZnSe alloyed core/shell QDs, which should have reduced Fröhlich EPC because the hole rather than the electron is extended into the shell, show nearly identical Raman cross sections and overtone to fundamental ratios to pure CdSe QDs (see Supporting Information). Thus, although the size-dependent CdSe QD data were adequately explained by invoking a purely Fröhlich mechanism,[35] this mechanism appears inadequate to describe EPC in core/shell QDs.

The other main mechanism for EPC in semiconductors is deformation potential coupling, a short-range effect that results from the changes in bond order, and therefore bond length, upon exciting an electron from the valence band to the conduction band. Acoustic phonons can be strongly Franck−Condon active *via* the volume deformation potential, which describes the shift in the band gap energy upon uniform expansion or compression of all bonds. There is no net volume change associated with motion along an optical phonon coordinate, and, as discussed in the Supporting Information of ref 35, this mechanism should be a negligible source of EPC. This mechanism also predicts strong size dependence to the EPC, contrary to the experimental results. However, the local distortion of the atoms within the unit cell by an optical phonon also gives rise to what is known as the optical deformation potential.[37,54−59] This interaction couples the optical phonons only to the hole (valence band) wave functions; the interaction with the electron wave function is zero by symmetry. The fact that every system we have examined appears to have about the same EPC for the CdSe LO phonons seems to support a mechanism involving only the hole wave function. The large effective mass localizes the 1S hole function near the center of the particle in both pure CdSe and core/shell QDs, and if the coupling involved the hole only, it would be fairly insensitive to QD size or the presence of a shell. However, the optical deformation potential generates Raman intensity by coupling the components of the valence band,[58,59] and the valence band fine structure is should be strongly dependent on QD size and crystal structure (wurtzite *vs* zinc blende).[60] In contrast, the resonance Raman-determined EPCs are nearly independent of these properties.[34,39] Accordingly, this seems unlikely to be a dominant source of EPC in CdSe QDs.

Surface charging has long been suggested as a mechanism for enhancing EPC in semiconductor quantum dots based partly on smaller EPCs inferred from femtosecond pump−probe experiments compared with resonance Raman.[61,62] The very strong increase in the Raman cross sections near the absorption onset (Figures 5 and 6 and refs 34, 35, and 63) clearly argues that the Raman enhancement arises from the same transition responsible for the lowest-energy absorption band, so we focus on the effect of surface charges on the $1S_e-1S_{3/2}$ excitonic transition. A positive or negative charge on the surface generates a static electric field that acts to mix some amount of P-type character into the S-type electron and hole wave functions. This generates a net charge separation between electron and hole and creates an additional photoinduced electric field that couples to optical phonons through the Fröhlich mechanism. In a core/shell QD, a surface charge is separated from the core by a shell of high dielectric constant. This results in a smaller electric field and a smaller effect on EPC of the core modes in a core/shell QD than in a pure CdSe QD. It is possible that surface charges increase the EPC for optical phonons above what it would be in neutral QDs and that this effect becomes weaker as the CdS shell becomes thicker, thereby approximately counteracting the increase in Fröhlich coupling with increased shell thickness that would be expected in neutral particles. Model calculations indicate that the magnitude of this effect may be adequate to explain the experimental results. However, this mechanism would require a rather fortuitous cancellation of effects, and

we have not been able to significantly change the resonance Raman spectra by placing charged ligands on the surface. We therefore consider this mechanism unlikely, but we cannot reject it.

We do not, at present, have a satisfactory explanation for the relative independence of the EPC in CdSe-based QDs to size and shell properties. As discussed above, the experimental trends go in the opposite direction to the predictions of the Fröhlich mechanism, but none of the alternative mechanisms that we have considered appear physically reasonable and consistent with the data. Further experiments and calculations are underway with the goal of understanding these results.

CONCLUSIONS

Quantitative analysis of the resonance Raman spectra and excitation profiles of CdSe/CdS core/shell quantum dots leads to three main conclusions. First, the electronic excitations that dominate the absorption at high energies, >4000 cm^{-1} above the lowest excitonic transition, involve a large contribution from transitions that are localized to either the CdSe core or the CdS shell, and not delocalized between core and shell. This is in contrast to the lowest energy transition, which is localized largely in the QD core. Second, the LO phonons consist of many different modes having slightly different frequencies. The lowest energy CdS modes are in proximity to the core/shell interface as a result of lattice strain and mode mixing effects. Third, the magnitude of the electron−phonon coupling for the optical phonons of the CdSe core is slightly reduced upon adding a CdS shell, contrary to the expectations of a Fröhlich coupling mechanism. Further studies are underway to explain this surprising result.

METHODS

Nearly spherical CdSe quantum dots (QDs) with the zincblende crystal structure, and CdSe/CdS core/shell structures having both "thin" and "thick" shells, were synthesized using a variation of the method described by Peng's group.[8] The bare cores had a first excitonic absorption maximum at 522 nm, while the "thin" and "thick" shells had excitonic maxima at 564 and 590 nm, respectively. From the maps presented in ref 38, the bare cores have a diameter of 2.7 nm, while the "thin" and "thick" shells are about 0.5 and 1.6 nm thick, respectively, corresponding to about 1.5 and 4.5 CdS monolayers.

The strong fluorescence from the as-synthesized QDs prevented us from obtaining Raman spectra at wavelengths near the lowest excitonic absorption. The fluorescence of the bare cores was largely quenched by ligand exchange with hexadecanethiol, a well-known hole acceptor. This ligand red-shifts the absorption spectrum of small CdSe QDs by 3−6 nm. For the core/shell structures, confinement of the hole to the core region made it necessary to use an electron acceptor to quench the fluorescence. Methyl viologen was used for the thin shells, but because of the tendency of the particles to aggregate and precipitate with this ionic electron acceptor, benzophenone was used for the thicker shells. The electron quenchers did not shift the absorption spectra and did not change the Raman spectra at higher excitation energies where fluorescence from the unquenched particles was not a serious interference.

Resonance Raman spectra were obtained and processed as described in ref 34. Excitation wavelengths from a variety of laser sources were employed: 410 and 430 nm from a frequency-doubled picosecond mode-locked Ti:sapphire laser (Spectra-Physics Tsunami), 457.9−514.5 nm from an argon-ion laser (Coherent Innova 90C-5), 532 nm from a frequency-doubled CW Nd laser (Spectra-Physics Millennia V), and 543.5−632.8 nm from He−Ne lasers (Coherent and Melles Griot). QDs were dissolved in chloroform at concentrations of 5−30 μM and placed in 1 mm path length cuvettes which were translated continuously under the laser beam (~0.5 mW focused with a 10× objective) to avoid local heating or photoinduced changes. Frequency calibration and absolute Raman cross-sectional calculations were performed using the Raman lines of chloroform as internal standards. Raman spectra were obtained for both parallel and perpendicular polarizations for excitation wavelengths of 543.5 nm and below; for the three longest wavelengths, only the parallel polarization was used. Computational modeling of the experimental absorption spectra and resonance Raman excitation profiles was carried out as described in our previous study of CdSe.[34]

Conflict of Interest: The authors declare no competing financial interest.

Acknowledgment. This work was supported by NSF Grant No. CHE-1112192. The force field described in the Supporting Information was developed by Charlene Bwrede and supported by NSF-REU Grant No. DMR-1359406. Youhong Zeng synthesized the CdSe/ZnSe core/shell QDs discussed in the Supporting Information.

Supporting Information Available: The Supporting Information is available free of charge on the ACS Publications website at DOI: 10.1021/acsnano.5b02230.

Alternative modeling of the Raman excitation profiles to determine EPC; calculations of EPC for CdSe and CdSe/CdS QDs with the Fröhlich mechanism; absorption and resonance Raman spectra of CdSe/ZnSe core/shell QDs (PDF)

REFERENCES AND NOTES

1. Lu, L.; Xu, X.-L.; Liang, W.-T.; Lu, H.-F. Raman Analysis of CdSe/CdS Core-Shell Quantum Dots with Different CdS Shell Thickness. *J. Phys.: Condens. Matter* **2007**, *19*, 406221.
2. Chilla, G.; Kipp, T.; Menke, T.; Heitmann, D.; Nikolic, M.; Fromsdorf, A.; Kornowski, A.; Forster, S.; Weller, H. Direct Observation of Confined Acoustic Phonons in the Photoluminescence Spectra of a Single CdSe-CdS-ZnS Core-Shell-Shell Nanocrystal. *Phys. Rev. Lett.* **2008**, *100*, 057403.
3. Spinicelli, P.; Buil, S.; Quelin, X.; Mahler, B.; Dubertret, B.; Hermier, J.-P. Bright and Grey States in CdSe-CdS Nanocrystals Exhibiting Strongly Reduced Blinking. *Phys. Rev. Lett.* **2009**, *102*, 136801.
4. Zhang, J.; Zhang, X.; Zhang, J. Y. Dependence of Microstructure and Luminescence on Shell Layers in Colloidal CdSe/CdS Core/Shell Nanocrystals. *J. Phys. Chem. C* **2010**, *114*, 3904–3908.
5. Raino, G.; Stoferle, T.; Moreels, I.; Gomes, R.; Kamal, J. S.; Hens, Z.; Mahrt, R. F. Probing the Wave Function Delocalization in CdSe/CdS Dot-in-Rod Nanocrystals by Time- and Temperature-Resolved Spectroscopy. *ACS Nano* **2011**, *5*, 4031–4036.
6. Cordones, A. A.; Scheele, M.; Alivisatos, A. P.; Leone, S. R. Probing the Interaction of Single Nanocrystals with Inorganic Capping Ligands: Time-Resolved Fluorescence from CdSe−CdS Quantum Dots Capped with Chalcogenidometalates. *J. Am. Chem. Soc.* **2012**, *134*, 18366–18373.

7. Fernee, M. J.; Sinito, C.; Louyer, Y.; Potzner, C.; Nguyen, T.-L.; Mulvaney, P.; Tamarat, P.; Lounis, B. Magneto-Optical Properties of Trions in Non-Blinking Charged Nanocrystals Reveal an Acoustic Phonon Bottleneck. *Nat. Commun.* **2012**, *3*, 1287.
8. Nan, W.; Niu, Y.; Qin, H.; Cui, F.; Yang, Y.; Lai, R.; Lin, W.; Peng, X. Crystal Structure Control of Zinc-Blende CdSe/CdS Core/Shell Nanocrystals: Synthesis and Structure-Dependent Optical Properties. *J. Am. Chem. Soc.* **2012**, *134*, 19685–19693.
9. Pal, B. N.; Ghosh, Y.; Brovelli, S.; Laocharoensuk, R.; Klimov, V. I.; Hollingsworth, J. A.; Htoon, H. 'Giant' CdSe/CdS Core/Shell Nanocrystal Quantum Dots As Efficient Electroluminescent Materials: Strong Influence of Shell Thickness on Light-Emitting Diode Performance. *Nano Lett.* **2012**, *12*, 331–336.
10. Tschirner, N.; Lange, H.; Schliwa, A.; Biermann, A.; Thomsen, C.; Lambert, K.; Gomes, R.; Hens, Z. Interfacial Alloying in CdSe/CdS Heteronanocrystals: A Raman Spectroscopy Analysis. *Chem. Mater.* **2012**, *24*, 311–318.
11. Zhu, H.; Song, N.; Rodríguez-Córdoba, W.; Lian, T. Wave Function Engineering for Efficient Extraction of up to Nineteen Electrons from One CdSe/CdS Quasi-Type II Quantum Dot. *J. Am. Chem. Soc.* **2012**, *134*, 4250–4257.
12. Bae, W. K.; Padilha, L. A.; Park, Y.-S.; McDaniel, H.; Robel, I.; Pietryga, J. M.; Klimov, V. I. Controlled Alloying of the Core-Shell Interface in CdSe/CdS Quantum Dots for Suppression of Auger Recombination. *ACS Nano* **2013**, *7*, 3411–3419.
13. Beyler, A. P.; Marshall, L. F.; Cui, J.; Brokmann, X.; Bawendi, M. G. Direct Observation of Rapid Discrete Spectral Dynamics in Single Colloidal CdSe-CdS Core-Shell Quantum Dots. *Phys. Rev. Lett.* **2013**, *111*, 177401.
14. Chen, O.; Zhao, J.; Chauhan, V. P.; Cui, J.; Wong, C.; Harris, D. K.; Wei, H.; Han, H.-S.; Fukumura, D.; Jain, R. K.; et al. Compact High-Quality CdSe–CdS Core–Shell Nanocrystals with Narrow Emission Linewidths and Suppressed Blinking. *Nat. Mater.* **2013**, *12*, 445–451.
15. Dzhagan, V. M.; Valakh, M. Y.; Milekhin, A. G.; Yeryukov, N. A.; Zahn, D. R. T.; Cassette, E.; Pons, T.; Dubertret, B. Raman- and IR-Active Phonons in CdSe/CdS Core/Shell Nanocrystals in the Presence of Interface Alloying and Strain. *J. Phys. Chem. C* **2013**, *117*, 18225–18233.
16. Eshet, H.; Grünwald, M.; Rabani, E. The Electronic Structure of CdSe/CdS Core/Shell Seeded Nanorods: Type-I or Quasi-Type-II? *Nano Lett.* **2013**, *13*, 5880–5885.
17. Kunneman, L. T.; Zanella, M.; Manna, L.; Siebbeles, L. D. A.; Schins, J. M. Mobility and Spatial Distribution of Photoexcited Electrons in CdSe/CdS Nanorods. *J. Phys. Chem. C* **2013**, *117*, 3146–3151.
18. Liu, F.; Biadala, L.; Rodina, A. V.; Yakovlev, D. R.; Dunker, D.; Javaux, C.; Hermier, J.-P.; Efros, A. L.; Dubertret, B.; Bayer, M. Spin Dynamics of Negatively Charged Excitons in CdSe/CdS Colloidal Nanocrystals. *Phys. Rev. B: Condens. Matter Mater. Phys.* **2013**, *88*, 035302.
19. Shafran, E.; Borys, N. J.; Huang, J.; Talapin, D. V.; Lupton, J. M. Indirect Exciton Formation Due to Inhibited Carrier Thermalization in Single CdSe/CdS Nanocrystals. *J. Phys. Chem. Lett.* **2013**, *4*, 691–697.
20. She, C.; Bryant, G. W.; Demortiere, A.; Shevchenko, E. V.; Pelton, M. Controlling the Spatial Location of Photoexcited Electrons in Semiconductor CdSe/CdS Core/Shell Nanorods. *Phys. Rev. B: Condens. Matter Mater. Phys.* **2013**, *87*, 155427.
21. Silva, A. C. A.; Freitas Neto, E. S.; da Silva, S. W.; Morais, P. C.; Dantas, N. O. Modified Phonon Confinement Model and Its Application to CdSe/CdS Core-Shell Magic-Sized Quantum Dots Synthesized in Aqueous Solution by a New Route. *J. Phys. Chem. C* **2013**, *117*, 1904–1914.
22. Todescato, F.; Minotto, A.; Signorini, R.; Jasieniak, J. J.; Bozio, R. Investigation into the Heterostructure Interface of CdSe-Based Core-Shell Quantum Dots Using Surface-Enhanced Raman Spectroscopy. *ACS Nano* **2013**, *7*, 6649–6657.
23. Wu, K.; Rodrguez-Cordoba, W. E.; Liu, Z.; Zhu, H.; Lian, T. Beyond Band Alignment: Hole Localization Driven Formation of Three Spatially Separated Long-Lived Exciton States in CdSe/CdS Nanorods. *ACS Nano* **2013**, *7*, 7173–7185.
24. Biadala, L.; Siebers, B.; Gomes, R.; Hens, Z.; Yakovlev, D. R.; Bayer, M. Tuning Energy Splitting and Recombination Dynamics of Dark and Bright Excitons in CdSe/CdS Dot-in-Rod Colloidal Nanostructures. *J. Phys. Chem. C* **2014**, *118*, 22309–22316.
25. Cirillo, M.; Aubert, T.; Gomes, R.; Van Deun, R.; Emplit, P.; Biermann, A.; Lange, H.; Thomsen, C.; Brainis, E.; Hens, Z. "Flash" Synthesis of CdSe/CdS Core–Shell Quantum Dots. *Chem. Mater.* **2014**, *26*, 1154–1160.
26. Diroll, B. T.; Murray, C. B. High-Temperature Photoluminescence of CdSe/CdS Core/Shell Nanoheterostructures. *ACS Nano* **2014**, *8*, 6466–6474.
27. Qin, H.; Niu, Y.; Meng, R.; Lin, X.; Lai, R.; Fang, W.; Peng, X. Single-Dot Spectroscopy of Zinc-Blende CdSe/CdS Core/Shell Nanocrystals: Nonblinking and Correlation with Ensemble Measurements. *J. Am. Chem. Soc.* **2014**, *136*, 179–187.
28. Lupo, M. G.; Scotognella, F.; Zavelani-Rossi, M.; Lanzani, G.; Manna, L.; Tassone, F. Band-Edge Ultrafast Pump–Probe Spectroscopy of Core/Shell CdSe/CdS Rods: Assessing Electron Delocalization by Effective Mass Calculations. *Phys. Chem. Chem. Phys.* **2012**, *14*, 7420–7426.
29. Wu, K.; Hill, L. J.; Chen, J.; McBride, J. R.; Pavlopolous, N. G.; Richey, N. E.; Pyun, J.; Lian, T. Universal Length Dependence of Rod-to-Seed Exciton Localization Efficiency in Type I and Quasi-Type II CdSe@CdS Nanorods. *ACS Nano* **2015**, *9*, 4591–4599.
30. Giblin, J.; Protasenko, V.; Kuno, M. Wavelength Sensitivity of Single Nanowire Excitation Polarization Anisotropies Explained through a Generalized Treatment of Their Linear Absorption. *ACS Nano* **2009**, *3*, 1979–1987.
31. Li, J.; Wang, L.-W. First Principle Study of Core/Shell Structure Quantum Dots. *Appl. Phys. Lett.* **2004**, *84*, 3648–3650.
32. Fernée, M. J.; Littleton, B. N.; Cooper, S.; Rubinsztein-Dunlop, H.; Gomez, D. E.; Mulvaney, P. Acoustic Phonon Contributions to the Emission Spectrum of Single CdSe Nanocrystals. *J. Phys. Chem. C* **2008**, *112*, 1878–1884.
33. Kelley, A. M. Resonance Raman Overtone Intensities and Electron-Phonon Coupling Strengths in Semiconductor Nanocrystals. *J. Phys. Chem. A* **2013**, *117*, 6143–6149.
34. Baker, J. A.; Kelley, D. F.; Kelley, A. M. Resonance Raman and Photoluminescence Excitation Profiles and Excited-State Dynamics in CdSe Nanocrystals. *J. Chem. Phys.* **2013**, *139*, 024702.
35. Lin, C.; Gong, K.; Kelley, D. F.; Kelley, A. M. Size Dependent Exciton-Phonon Coupling in CdSe Nanocrystals Through Resonance Raman Excitation Profile Analysis. *J. Phys. Chem. C* **2015**, *119*, 7491–7498.
36. Rolo, A. G.; Vasilevskiy, M. I. Raman Spectroscopy of Optical Phonons Confined in Semiconductor Quantum Dots and Nanocrystals. *J. Raman Spectrosc.* **2007**, *38*, 618–633.
37. Vasilevskiy, M. I.; Trallero-Giner, C. Resonant Raman Scattering in Spherical Quantum Dots: II–VI *versus* III–V Semiconductor Nanocrystals. *Phys. Status Solidi B* **2010**, *247*, 1488–1491.
38. Gong, K.; Martin, J. E.; Shea-Rohwer, L. E.; Lu, P.; Kelley, D. F. Radiative Lifetimes of Zincblende CdSe/CdS Quantum Dots. *J. Phys. Chem. C* **2015**, *119*, 2231–2238.
39. Kelley, A. M.; Dai, Q.; Jiang, Z.-j.; Baker, J. A.; Kelley, D. F. Resonance Raman Spectra of Wurtzite and Zincblende CdSe Nanocrystals. *Chem. Phys.* **2013**, *422*, 272–276.
40. Myers, A. B.; Mathies, R. A. Resonance Raman Intensities: A Probe of Excited-State Structure and Dynamics. In *Biological Applications of Raman Spectroscopy*; Spiro, T. G., Ed.; Wiley: New York, 1987; Vol. 2, pp 1–58.
41. Kelley, A. M. Electron-Phonon Coupling in CdSe Nanocrystals from an Atomistic Phonon Model. *ACS Nano* **2011**, *5*, 5254–5262.
42. Lin, C.; Kelley, D. F.; Rico, M.; Kelley, A. M. The "Surface Optical" Phonon in CdSe Nanocrystals. *ACS Nano* **2014**, *8*, 3928–3938.
43. Zou, S. Z.; Weaver, M. J. Surface-Enhanced Raman Spectroscopy of Cadmium Sulfide/Cadmium Selenide Superlattices

Formed on Gold by Electrochemical Atomic-Layer Epitaxy. *Chem. Phys. Lett.* **1999**, *312*, 101–107.
44. Shiang, J. J.; Risbud, S. H.; Alivisatos, A. P. Resonance Raman Studies of the Ground and Lowest Electronic Excited State in CdS Nanocrystals. *J. Chem. Phys.* **1993**, *98*, 8432–8442.
45. Wu, Y.; Jin, S.; Ye, Y.; Wang, S.; Feng, Z.; Li, C. Charge-Sensitive Surface Optical Phonon in CdS Quantum Dots Studied by Resonant Raman Spectroscopy. *J. Phys. Chem. C* **2014**, *118*, 30269–30273.
46. Freitas Neto, E. S.; Dantas, N. O.; da Silva, S. W.; Morais, P. C.; Pereira-da-Silva, M. A.; Moreno, A. J. D.; Lopez-Richard, V.; Marques, G. E.; Trallero-Giner, C. Temperature-Dependent Raman Study of Thermal Parameters in CdS Quantum Dots. *Nanotechnology* **2012**, *23*, 125701.
47. Camacho, J.; Cantarero, A. Lattice Dynamics in Wurtzite Semiconductors: The Bond Charge Model of CdS. *Phys. Status Solidi B* **1999**, *215*, 181–187.
48. Gong, K.; Kelley, D. F. A Predictive Model of Shell Morphology in CdSe/CdS Core/Shell Quantum Dots. *J. Chem. Phys.* **2014**, *141*, 194704.
49. Norris, D. J., Electronic Structure in Semiconductor Nanocrystals: Optical Experiment. In *Nanocrystal Quantum Dots*, 2nd ed.; Klimov, V. I., Ed.; CRC Press: Boca Raton, FL, 2010; pp 63−96.
50. Sewall, S. L.; Cooney, R. R.; Kambhampati, P. Experimental Tests of Effective Mass and Atomistic Approaches to Quantum Dot Electronic Structure: Ordering of Electronic States. *Appl. Phys. Lett.* **2009**, *94*, 243116.
51. Fu, H. X.; Wang, L. W.; Zunger, A. Comparison of the k Center Dot p and the Direct Diagonalization Approaches for Describing the Electronic Structure of Quantum Dots. *Appl. Phys. Lett.* **1997**, *71*, 3433–3435.
52. Cho, B.; Peters, W. K.; Hill, R. J.; Courtney, T. L.; Jonas, D. M. Bulklike Hot Carrier Dynamics in Lead Sulfide Quantum Dots. *Nano Lett.* **2010**, *10*, 2498–2505.
53. Trinh, M. T.; Sfeir, M. Y.; Choi, J. J.; Owen, J. S.; Zhu, X. A Hot Electron−Hole Pair Breaks the Symmetry of a Semiconductor Quantum Dot. *Nano Lett.* **2013**, *13*, 6091–6097.
54. Potz, W.; Vogl, P. Theory of Optical-Phonon Deformation Potentials in Tetrahedral Semiconductors. *Phys. Rev. B: Condens. Matter Mater. Phys.* **1981**, *24*, 2025–2037.
55. Braun, D.; Ruhle, W. W.; Trallero-Giner, C. Spectroscopic Determination of the Optical Deformation-Potential Constant in Semiconductors. *Phys. Rev. Lett.* **1991**, *67*, 2335–2338.
56. Chernikov, A.; Bornwasser, V.; Koch, M.; Chatterjee, S.; Bottge, C. N.; Feldtmann, T.; Kira, M.; Koch, S. W.; Wassner, T.; Lautenschlager, S.; et al. Phonon-Assisted Luminescence of Polar Semiconductors: Frohlich Coupling *versus* Deformation-Potential Scattering. *Phys. Rev. B: Condens. Matter Mater. Phys.* **2012**, *85*, 035201.
57. Dargys, A. Hole Spin Relaxation: Optical Deformation Potential Scattering. *Semicond. Sci. Technol.* **2005**, *20*, 733–739.
58. Shiang, J. J.; Wolters, R. H.; Heath, J. R. Theory of Size-Dependent Resonance Raman Intensities in InP Nanocrystals. *J. Chem. Phys.* **1997**, *106*, 8981–8994.
59. Hamma, M.; Miranda, R. P.; Vasilevskiy, M. I.; Zorkani, I. Calculation of the Huang−Rhys Parameter in Spherical Quantum Dots: The Optical Deformation Potential Effect. *J. Phys.: Condens. Matter* **2007**, *19*, 346215.
60. Efros, A. L.; Rosen, M.; Kuno, M.; Nirmal, M.; Norris, D. J.; Bawendi, M. Band-Edge Exciton in Quantum Dots of Semiconductors With a Degenerate Valence Band: Dark and Bright Exciton States. *Phys. Rev. B: Condens. Matter Mater. Phys.* **1996**, *54*, 4843–4856.
61. Krauss, T. D.; Wise, F. W. Raman-Scattering Study of Exciton-Phonon Coupling in PbS Nanocrystals. *Phys. Rev. B: Condens. Matter Mater. Phys.* **1997**, *55*, 9860–9865.
62. Sagar, D. M.; Cooney, R. R.; Sewall, S. L.; Dias, E. A.; Barsan, M. M.; Butler, I. S.; Kambhampati, P. Size Dependent, State-Resolved Studies of Exciton-Phonon Couplings in Strongly Confined Semiconductor Quantum Dots. *Phys. Rev. B: Condens. Matter Mater. Phys.* **2008**, *77*, 235321.
63. Alivisatos, A. P.; Harris, T. D.; Carroll, P. J.; Steigerwald, M. L.; Brus, L. E. Electron-Vibration Coupling in Semiconductor Clusters Studied by Resonance Raman Spectroscopy. *J. Chem. Phys.* **1989**, *90*, 3463–3468.